Materials Science & Engineering C 85 (2018) 79–87

Contents lists available at ScienceDirect

Materials Science & Engineering C

journal homepage: www.elsevier.com/locate/msec

Biomimetic polyurethane/TiO_2 nanocomposite scaffolds capable of promoting biomineralization and mesenchymal stem cell proliferation

Qingxia Zhu[a,b], Xiaofei Li[a], Zhaobo Fan[a], Yanyi Xu[a], Hong Niu[a], Chao Li[a], Yu Dang[a], Zheng Huang[a], Yun Wang[c], Jianjun Guan[a,*]

[a] Department of Materials Science and Engineering, The Ohio State University, 2041 College Road, Columbus, OH 43210, USA
[b] Department of Materials Science and Engineering, Jingdezhen Ceramic Institute, Jiangxi 333001, China
[c] Division of Periodontology, The Ohio State University, 305 W. 12th Avenue, Columbus, OH 43210, USA

ARTICLE INFO

Keywords:
Nanocomposite
Polyurethane
TiO_2 nanoparticle
Mesenchymal stem cells
Biocompatibility

ABSTRACT

Scaffolds with extracellular matrix-like fibrous morphology, suitable mechanical properties, biomineralization capability, and excellent cytocompatibility are desired for bone regeneration. In this work, fibrous and degradable poly(ester urethane)urea (PEUU) scaffolds reinforced with titanium dioxide nanoparticles ($nTiO_2$) were fabricated to possess these properties. To increase the interfacial interaction between PEUU and $nTiO_2$, poly (ester urethane) (PEU) was grafted onto the $nTiO_2$. The scaffolds were fabricated by electrospinning and exhibited fiber diameter of < 1 μm. SEM and EDX mapping results demonstrated that the PEU modified $nTiO_2$ was homogeneously distributed in the fibers. In contrast, severe agglomeration was found in the scaffolds with unmodified $nTiO_2$. PEU modified $nTiO_2$ significantly increased Young's modulus and tensile stress of the PEUU scaffolds while unmodified $nTiO_2$ significantly decreased Young's modulus and tensile stress. The greatest reinforcement effect was observed for the scaffold with 1:1 ratio of PEUU and PEU modified $nTiO_2$. When incubating in the simulated body fluid over an 8-week period, biomineralization was occurred on the fibers. The scaffolds with PEU modified $nTiO_2$ showed the highest Ca and P deposition than pure PEUU scaffold and PEUU scaffold with unmodified $nTiO_2$. To examine scaffold cytocompatibility, bone marrow-derived mesenchymal stem cells were cultured on the scaffold. The PEUU scaffold with PEU modified $nTiO_2$ demonstrated significantly higher cell proliferation compared to pure PEUU scaffold and PEUU scaffold with unmodified $nTiO_2$. The above results demonstrate that the developed fibrous nanocomposite scaffolds have potential for bone tissue regeneration.

1. Introduction

Self-regeneration of critical size bone defects caused by trauma, tumor removal, and infection remains challenging in clinical settings [1–3]. Scaffolds have been widely used to aid the regeneration. A typical scaffold should have appropriate porosity to allow cell ingrowth, be osteoconductive, and possess suitable mechanical properties [1–3]. Among different types of scaffolds, those mimicking the properties of bone tissue extracellular matrix (ECM) have been considered as promising candidates [4–7]. These scaffolds can accelerate the regeneration by preventing fibrous encapsulation, promoting osseointegration, and stimulating cell infiltration, proliferation and osteogenic differentiation [4–8].

Bone is a hard tissue that also has high toughness and tensile strength. To fabricate scaffolds with suitable toughness, flexible polymers such as polyurethane and polycaprolactone can be used [9–44]. The resulting scaffolds generally have higher toughness than those based on stiffer polymers such as polylactide and polyglycolide. Biodegradable polyurethane is a class of polymer that has attracted great attention in the biomaterials community due to its excellent biocompatibility and robust mechanical properties. Porous thermoplastic and thermoset polyurethane scaffolds have been utilized for bone regeneration in animal and preclinical studies [9–29]. The scaffolds with tailored chemical and mechanical properties can promote osteogenic cells to populate and differentiate within the scaffolds, thus stimulating bone regeneration [25–29]. To further augment the regeneration, growth factors such as BMP-2 and PDGF have been loaded into polyurethane scaffolds [28,45–47]. One of the limitations for biodegradable polyurethane scaffolds is that their modulus and tensile strength are much lower than those of the bone tissue. Increasing these properties is expected to make polyurethane scaffolds more suitable for bone regeneration. An effective approach is to use stiffer soft segment during

* Corresponding author.
E-mail address: guan.21@osu.edu (J. Guan).

https://doi.org/10.1016/j.msec.2017.12.008
Received 26 June 2017; Received in revised form 24 August 2017; Accepted 7 December 2017
Available online 18 December 2017

the synthesis. For example, replacing polycaprolactone with polyhydroxybutyrate can largely increase polyurethane Young's modulus and tensile strength [48–52]. However, this approach may simultaneously compromise toughness of the polymers.

Polyurethane composite scaffolds may retain toughness of the polyurethane while increasing modulus and tensile strength. Microspheres and nanoparticles can be incorporated into polyurethane scaffolds during the fabrication, such as hydroxyapatite [14,53,54], carbon nanotubes [55–57], and titanium dioxide (TiO_2) [58,59]. These inorganic materials are much stronger and stiffer than polymers. Compared to microspheres, nanoparticles may better reinforce polyurethanes because of their higher surface area-to-volume ratio [60]. TiO_2 nanoparticles are attractive for polymer reinforcement especially in dental applications [61–63]. These nanoparticles have good biocompatibility and antibacterial property [61–63]. In addition, they can suppress immune response which commonly occurs after scaffold implantation [64]. In this work, we took advantage of these properties to fabricate TiO_2 nanoparticles-reinforced polyurethane scaffolds. A major limitation of using unmodified TiO_2 nanoparticles to reinforce polymers is the uneven distribution, which compromises the reinforcement effect [65]. In addition, the nanoparticles may readily leach out from the scaffolds when their interactions with polymers are weak [65]. The released nanoparticles may be intaken by cells causing potential damage [66]. To address these limitations, approaches such as surface modification of TiO_2 nanoparticles, [65] and increase of polymer polarity [67] have been developed to augment the physical interactions of the nanoparticles and polymers. In this work, we hypothesized that chemical conjugation of polymers to the TiO_2 nanoparticles can better increase the interactions than simply modifying either the nanoparticles or polymers, thus efficiently increasing scaffold modulus and tensile strength, and decreasing nanoparticle release.

Bone tissue ECM is a nanocomposite consisting of collagen fibers and hydroxyapatite nanoparticles. Thus, scaffolds with fibrous morphology and biomineralization capability are desired for bone regeneration. To fabricate scaffolds with fibrous morphology, commonly used techniques include thermally induced phase separation [68–71], and electrospinning [72–75]. Thermally induced phase separation technique generates fibers with diameter ranging from few to 100 nm depending on the phase separation temperature and solution concentration [68–71]. Electrospinning of polymer solution is a more convenient approach to fabricate fibrous scaffolds. The resulting scaffolds typically have fiber diameters in the range of 10–1000 nm, within the range of fibrous ECM [72–75]. A major advantage of electrospinning is that reinforcement nanoparticles can be readily incorporated into the fibers during fabrication by mixing with polymer solutions [76]. In this work, we electrospun polyurethane scaffolds with TiO_2 nanoparticles in the fibers. Previous study demonstrated that TiO_2 surface with nanostructure has the ability to promote apatite formation [8]. It is hypothesized that the TiO_2 nanoparticles impart the scaffolds with biomineralization capability. We investigated the capability of TiO_2 nanoparticles in improving scaffold mechanical properties, promoting biomineralization, and supporting osteogenic cell proliferation.

2. Materials and methods

2.1. Materials

All chemicals were purchased from Sigma-Aldrich unless otherwise stated. Hexamethylene diisocyanate (HMDI) was purified by vacuum distillation. Polycaprolactone (PCL) diol with an average molecular weight of 2000 g/mol, and dimethylolpropionic acid (DMPA) were vacuum dried overnight at 60 °C before use. TiO_2 nanoparticles comprised of 50% anatase and 50% rutile crystal forms. The average particle size and purity were 21 nm and 99.9%, respectively. Anhydrous toluene, dimethylformamide (DMF), and isopropanol were used as received.

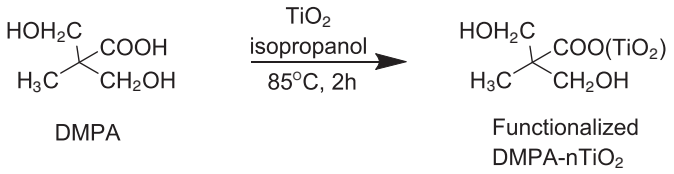

Fig. 1. Synthesis of DMPA functionalized TiO_2 nanoparticles (DMPA-nTiO_2).

2.2. Functionalization of TiO_2 nanoparticles with reactive hydroxyl groups

TiO_2 nanoparticles were reacted with DMPA to introduce hydroxyl groups (Fig. 1) following a previous report [65]. DMPA was dissolved in 2-propanol. The nanoparticles were then dispersed in the DMPA solution. After ultrasonic agitation for 5 min, the mixture was reacted at 80 °C for 12 h under constant stirring with the protection of nitrogen gas. The molar ratio of DMPA to nTiO_2 was controlled at 2.4. After reaction, the nanoparticles were collected by centrifugation at 10000 rpm, and then washed with methanol for 3 times to remove the unreacted DMPA.

2.3. Synthesis of poly(ester urethane) (PEU) grafted TiO_2, and poly(ester urethane)urea (PEUU)

The PEU grafted TiO_2 nanoparticles (PEU-g-nTiO_2) were synthesized by a two-step approach (Fig. 2). In the first step, HMDI and PCL diol were dissolved in a mixture of DMF/toluene at 1:1 volume ratio. The molar ratio of HMDI and PCL diol was 2:1. Stannous octoate was then added. The reaction was conducted at 85 °C for 2 h with the protection of nitrogen gas. In the second step, the DMPA functionalized nTiO_2 was added to the above solution. The molar ratio of HMDI and the functionalized nTiO_2 was 1:1. The reaction was conducted at 80 °C for 4 h. The mixture was then centrifuged followed by washing with DMF/toluene for 3 times. The PEU-g-nTiO_2 was finally vacuum dried at 40 °C. To confirm the conjugation of PEU, the material was characterized by FT-IR.

PEUU was synthesized using PCL as soft segment, and HMDI and putrescine as hard segment following our established protocols [75,77]. The molar ratio of PCL diol, HMDI and putrescine was controlled at 1/2/1. In brief, PCL diol was dissolved in DMSO to form a solution. HMDI was then added under the protection of nitrogen gas. After addition of stannous octoate, the reaction was conducted at 80 °C in an oil bath for 3 h to form prepolymer. The solution was cooled down to room temperature. Putrescine solution in DMSO was then added dropwise to the prepolymer solution for chain extension. The mixture was stirred at room temperature overnight. The polymer solution was precipitated in cold NaCl solution. After immersing in the DI water for 24 h, the polymer was vacuum dried at 60 °C.

2.4. Fabrication of fibrous PEUU scaffolds reinforced with PEU-g-nTiO_2

The fibrous scaffolds were fabricated by electrospinning. PEUU was dissolved in 1,1,1,3,3,3-hexafluoro-2-propanol (HFIP) to form a 6% solution. PEU-g-TiO_2 was then added to the solution. The mixture was sonicated to allow particles to uniformly distribute in the solution. The ratio of PEUU and PEU-g-TiO_2 was controlled at 1/1, 1/2, and 2/1 wt%, respectively. The mixture was charged at + 15 kV. The flow rate was 1 mL/h. The fibers were collected on a rotating mandrel with rotation speed of 1000 rpm, and charged at − 10 kV. The resulting scaffolds (abbreviated as PEU-g-TiO_2/PEUU) had a thickness of ~100 μm. Pure PEUU scaffold, and PEUU scaffold with unmodified TiO_2 nanoparticles (ratio of 1:1, abbreviated as nTiO_2/PEUU) were also fabricated to serve as controls.

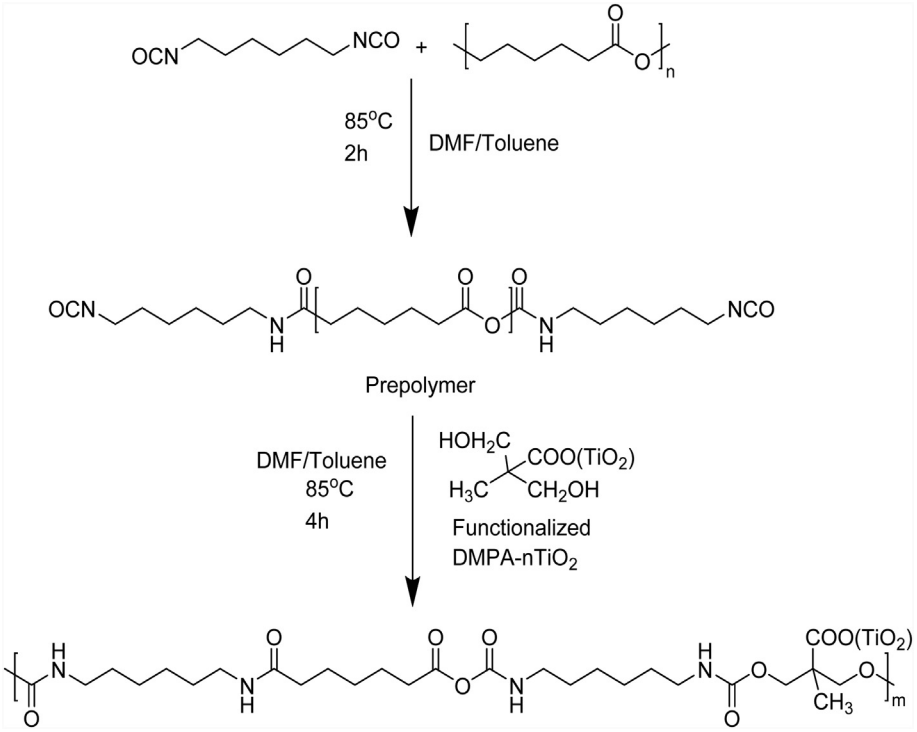

Fig. 2. Synthesis of degradable polyurethane conjugated with TiO_2 nanoparticles (PEU-g-nTiO_2).

2.5. Characterization of PEUU scaffolds reinforced with PEU-g-nTiO_2

Morphology of the scaffolds was characterized by a LEO 1530 scanning electron microscopy (SEM). The bulk composition was analyzed using energy-dispersive x-ray spectroscopy (EDX) attached to the SEM. FT-IR spectra were recorded on a Nicolet Magna-IR 750 spectrometer. To measure mechanical properties, dog bone-shaped die with ~20 mm gauge length and ~2 mm gauge width were used to cut 4–5 specimens from each scaffold. The specimens were immersed in 37 °C water for 24 h before test. The tensile testing was performed on a TestResources 1000R load frame (model 1322) equipped with a 222.4 N load cell and a 37 °C water bath [75,77]. A cross-head speed of 10 mm/min was used.

2.6. Biomineralization of PEUU scaffolds reinforced with PEU-g-nTiO_2

PEUU, nTiO_2/PEUU, and PEU-g-nTiO_2/PEUU scaffolds were used for the assessment of biomineralization property. The samples were weighted and then immersed in a simulated body fluid (SBF) at 37 °C. SBF was prepared by dissolving 10.806 g NaCl, 0.852 g Na_2CO_3, 1.008 g $NaHCO_3$, 0.144 g Na_2SO_4, 0.450 g KCl, 0.351 g K_2HPO_4, 0.622 g $MgCl_2{\cdot}6H_2O$, 200 mL of 0.2 M NaOH solution, and 0.586 g $CaCl_2$ and 34.784 g HEPES in 1 L of DI water [78]. The inorganic ion concentrations in SBF were equal to those of human blood plasma [78]. After 1, 2, 4, and 8 weeks of incubation, samples ($n = 5$ for each scaffold type at each time point) were collected, freeze dried, and weighted. Weight change was then quantified. To confirm the biomineralization, EDX was used to characterize the scaffolds.

2.7. Mesenchymal stem cell growth on PEUU scaffolds reinforced with PEU-g-nTiO_2

To evaluate the ability of PEUU scaffolds reinforced with PEU-g-nTiO_2 to support cell growth, rat bone marrow-derived mesenchymal stem cells (MSCs) were seeded on the scaffolds. PEUU and nTiO_2/PEUU scaffolds were used as controls. MSCs were cultured in a T-175 flask using Dulbecco's Modified Eagle Medium (DMEM) supplemented with 20% FBS, 2% L-glutamine and 1% penicillin/streptomycin as culture medium [79,80]. The scaffolds were punched into 6 mm diameter disks. After sterilizing under UV irradiation for 1 h in a laminar flow hood, the disks were placed in a 96-well tissue culture plate. MSCs were seeded onto each disk at a density of 2×10^5 cells/mL. After 1, 3, and 7 days of culture under normal conditions (21% O_2, 5% CO_2), double-stranded DNA (dsDNA) content of the live cells in each sample was measured using PicoGreen assay (Invitrogen) [79,80].

2.8. Statistical analysis

One way ANOVA test was utilized for data analysis. Data were presented as mean ± standard deviation. Statistical significance was defined as $p < 0.05$.

3. Results and discussion

3.1. Synthesis of PEU-g-nTiO_2

TiO_2 nanoparticle was first functionalized with DMPA to introduce hydroxyl groups onto the surface before grafting PEU. These hydroxyl groups can readily react with isocyanate groups. The reaction of DMPA and nTiO_2 is occurred between carboxyl groups of DMPA and Ti of nTiO_2 by forming bidentate chelating type coordination bonding [81]. To graft PEU onto the functionalized TiO_2 nanoparticles, PEU prepolymer with isocyanate groups was first prepared by reacting PCL diol with HMDI at a molar ratio of 1:2. The use of PCL allows the PEU to be degradable. Successful synthesis of PEU-g-nTiO_2 was confirmed by FTIR spectrum that exhibited characteristic peaks of PEU and TiO_2 (Fig. 3). The absorption at 643 cm^{-1} is from nTiO_2. The carbonyl peak at 1725 cm^{-1} is from urethane group. All of the isocyanate groups in the prepolymer were reacted with hydroxyl groups introduced onto the nTiO_2 surface since there is no isocyanate peak at 2265 cm^{-1}. Consistent with previous report, [65] the coordination bonding between DMPA and nTiO_2 is not obvious in the spectrum, possibly because the absorption level of Ti–O–C coordination is significantly small compared to that of the bonds in PEU.

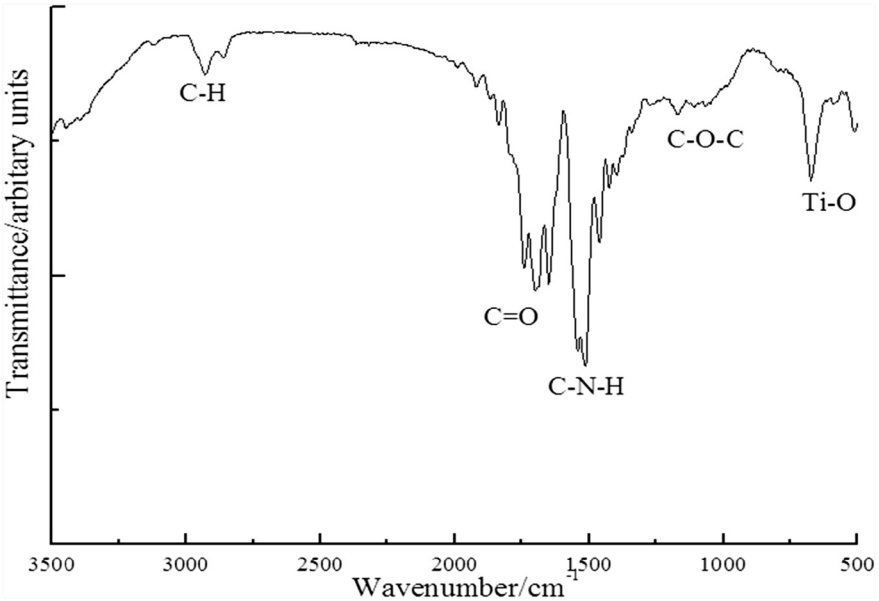

Fig. 3. FTIR spectrum of synthesized PEU-g-nTiO$_2$.

3.2. Fibrous nanocomposite scaffold fabrication

Fibrous scaffolds based on PEUU and PEU-g-nTiO$_2$ were fabricated by electrospinning. The PEUU was synthesized using the same soft segment and diisocyanate as PEU. Our previous study demonstrated that this polymer supported the growth of cardiosphere-derived cells [75]. HFIP was used as a solvent for PEUU. The benefit of using this high polarity solvent is that it allowed PEU-g-nTiO$_2$ to evenly and stably suspend in the PEUU solution, thus facilitating the fabrication of fibers with uniform distribution of nTiO$_2$.

The fabricated PEUU scaffold without nTiO$_2$ or PEU-g-nTiO$_2$ assumed smooth fibers with a diameter < 1 μm (Fig. 4a). The scaffolds based on unmodified nTiO$_2$ and PEUU (nTiO$_2$/PEUU) exhibited both fibers and beads (Fig. 4b). EDX analysis was performed to determine the distribution of nTiO$_2$. Fig. 5 demonstrated that nanoparticles were not uniformly distributed in the scaffolds, and beads were nanoparticle aggregation. It is likely that unmodified nTiO$_2$ aggregated during the fabrication due to poor interactions between nTiO$_2$ and PEUU. The modification of nTiO$_2$ with PEU (PEU-g-nTiO$_2$) increased the interfacial interaction of the nanoparticles and PEUU. This allowed nanoparticles to stably suspend in the solution during scaffold fabrication. As a result, the scaffolds contained only fibers without beads (Fig. 4d–e). EDX analysis confirmed that nanoparticles were evenly distributed in the scaffolds (Fig. 5). Scaffold fiber morphology was dependent on the ratio of PEU-g-nTiO$_2$ to PEUU. When the ratio was 1:2, the fibers were smooth. The increase of the ratio to 1:1 and 2:1 led to forming more rough fibers (Fig. 4e).

3.3. Scaffold mechanical properties

One of the purposes in using nTiO$_2$ is to reinforce the PEUU scaffolds thus increasing both Young's modulus and tensile strength for improved performance during bone regeneration. The pure PEUU scaffold had Young's modulus and tensile strength of 31.8 ± 2.3 and 34.3 ± 0.9, respectively. Simply mixing unmodified nTiO$_2$ and PEUU (nTiO$_2$/PEUU scaffold) did not show reinforcement effect. Instead, both

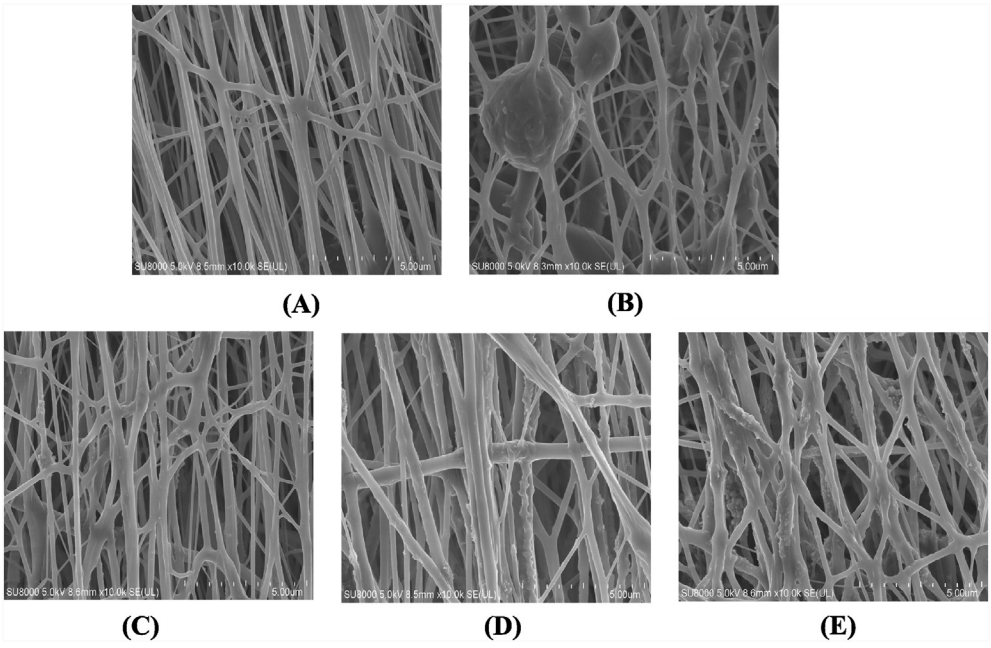

Fig. 4. Morphology of the electrospun scaffolds. (A) PEUU; (B) nTiO$_2$/PEUU; (C) PEU-g–nTiO$_2$/PEUU = 1:2; (D) PEU-g–nTiO$_2$/PEUU = 1:1; and (E) PEU-g–nTiO$_2$/PEUU = 2:1.

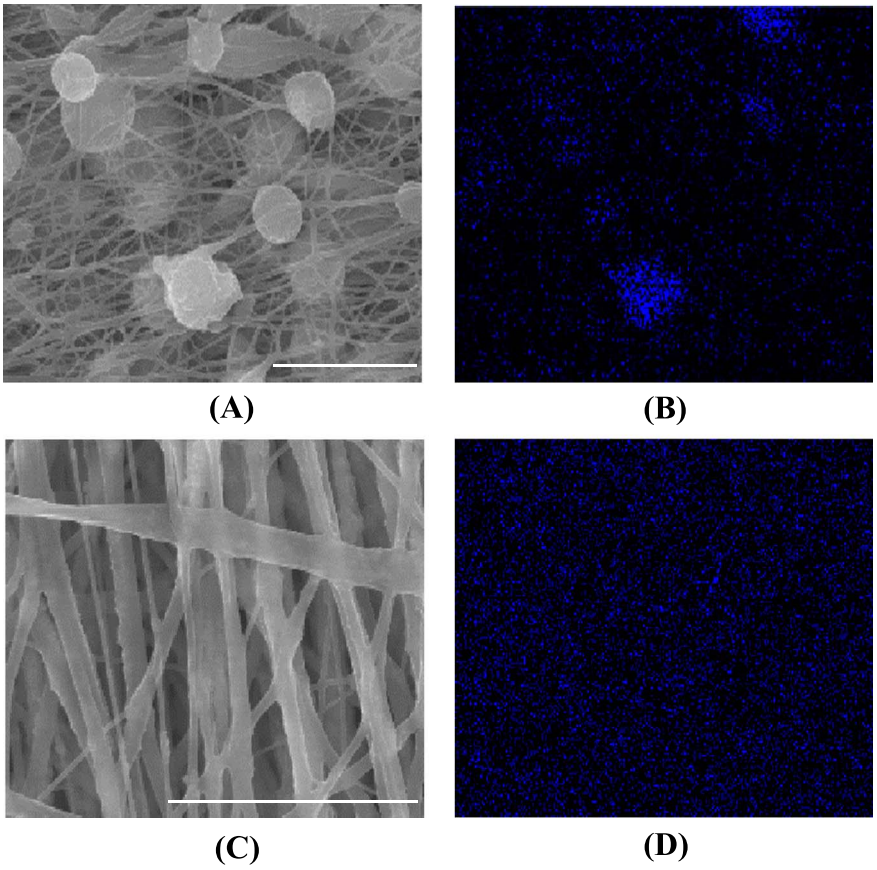

Fig. 5. SEM images (A, C) and corresponding EDX analysis of Ti distribution in the scaffolds (B, D). (A, B) $nTiO_2$/PEUU; (C, D) PEU-g–$nTiO_2$/PEUU = 2/1. Scale bar = 5 μm.

Young's modulus and tensile strength were significantly decreased compared with PEUU scaffold ($p < 0.001$). This is likely due to the low interfacial interaction between $nTiO_2$ and PEUU. It led to the aggregation of $nTiO_2$ in the solution during the scaffold fabrication process. The scaffolds therefore had $nTiO_2$ aggregates attached to the fibers (Fig. 4b and Fig. 5a), which cannot efficiently dissipate external force. For those nanoparticles that are in the fibers, even they can dispense uniformly, the weak interfacial interaction between PEUU cannot effectively reinforce the scaffold.

Modification of $nTiO_2$ with PEU (PEU-g-$nTiO_2$) can increase its interfacial interaction with PEUU because of the strong hydrogen bonding between urethane groups and urethane-urea groups in both polymers. This resulted in the reinforcement effect. Fig. 6 demonstrated that adding PEU-g-$nTiO_2$ into the PEUU scaffolds significantly increased Young's modulus compared to the pure PEUU scaffold when the ratio of PEU-g-$nTiO_2$ and PEUU was ranged from 1:2 to 2:1 ($p < 0.01$). The highest Young's modulus was for the scaffold with the ratio of 1:1 where it was 48.8 ± 3.2 MPa, a 53.5% of increase over pure PEUU scaffold. For the tensile strength, the scaffolds with PEU-g-$nTiO_2$/PEUU ratios of 1:2 and 1:1 were significantly higher than pure PEUU scaffold ($p < 0.05$) while the scaffold with the ratio of 2:1 showed similar value. The decrease of Young's modulus and tensile strength when the PEU-g-$nTiO_2$/PEUU ratio was increased from 1:1 to 2:1 is probably attributed to the decrease of interfacial interaction between PEUU and PEU when the content of PEU-g-$nTiO_2$ is higher than PEUU. It is also possible that PEU-g-$nTiO_2$ cannot efficiently distribute in the PEUU

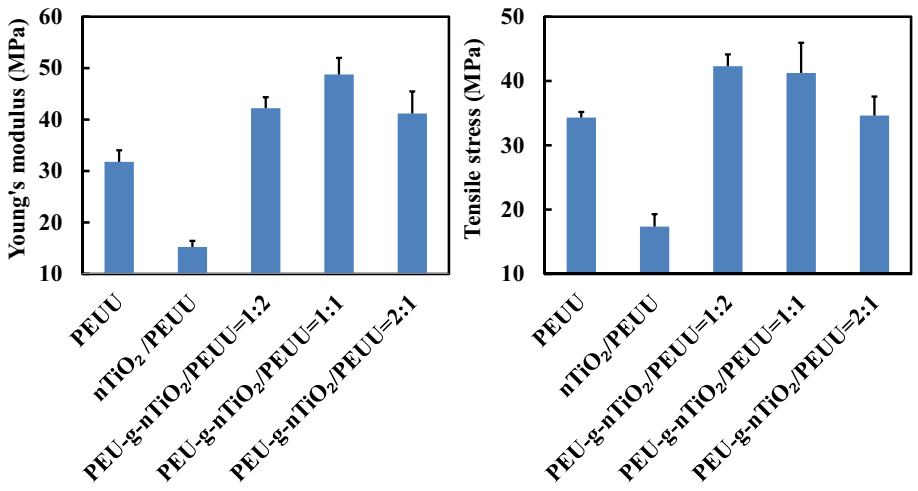

Fig. 6. Mechanical properties of electrospun scaffolds with and without reinforcement with PEU-gnTiO_2.

fibers when its content is high. Similar trend was found for collagen scaffolds reinforced with carbon nanotubes [82].

3.4. Scaffold biomineralization

Biomineralization is critical during bone regeneration. Scaffolds capable of stimulating biomineralization may be able to promote the regeneration [8]. The developed fibrous scaffolds have high surface-area-to-volume ratio, thus may facilitate the biomineralization. To investigate the biomineralization capability of TiO_2 nanoparticles reinforced PEUU scaffold, PEU-g-nTiO_2/PEUU = 1:1 was used since it had the highest Young's modulus. The scaffold was incubated in SBF for 8 weeks. Controls were PEUU and nTiO_2/PEUU scaffolds. All scaffolds showed slight weight loss after 1 week of incubation ($p > 0.05$ for each scaffold). It is possible that PEUU degradation-induced weight loss is greater than biomineralization-induced weight gaining during this period. The PEUU scaffold exhibited continuous weight loss for 4 weeks. Significant net weight gaining was observed only after 8 weeks ($p < 0.05$, week 4 vs. week 8), indicating that biomineralization was dominated for PEUU after 4 weeks. The nTiO_2/PEUU scaffold demonstrated net weight gaining after 4 weeks, earlier than PEUU scaffold. After 8 weeks of incubation, the scaffold gained ~13% of weight, significantly greater than the original weight ($p < 0.05$, week 0 vs. week 8). These results suggest that TiO_2 nanoparticles in the scaffold accelerated the biomineralization. This is consistent with previous studies where TiO_2 containing materials promoted the absorption of Ca^{2+} and PO_4^{3-} [83].

The PEU-g-nTiO_2/PEUU scaffold showed net weight gaining only after 2 weeks of incubation, sooner than nTiO_2/PEUU scaffold. After 8 weeks, the net weight gaining was 10% ($p < 0.05$ for weight of week 0 vs. weight of week 8). The Ca and P containing ions were deposited uniformly in the PEU-g-nTiO_2/PEUU scaffold (Fig. 8), attributing to the even distribution of TiO_2 nanoparticles (Fig. 5). Elemental content of Ca and P analyzed from EDX mapping is listed in Table 1. Consistent with weight change results in Fig. 7, the PEU-g-nTiO_2/PEUU scaffold had the highest Ca and P deposition. In addition, the nTiO_2/PEUU scaffold demonstrated greater Ca and P deposition than PEUU scaffold. The above results suggest that PEU modification stimulated nTiO_2 biomineralization. The PEU grafted onto the nanoparticles is based on polycaprolactone and HMDI. The chain length of PEU should be shorter than that of PEUU as no chain extension reaction was performed for it. Therefore, PEU possibly degraded faster than PEUU. The hydrolysis of PCL chain may leave –COOH groups on the nTiO_2 surface, which then attract cationic species like Ca^{2+} to deposit.

3.5. Mesenchymal stem cell growth on scaffolds

Scaffolds for bone regeneration can be implanted alone to allow endogenous cells including osteoblasts and stem cells to induce regeneration. They can also be transplanted together with osteogenic cells to direct the regeneration. In both approaches, it is necessary for the scaffolds to support cell proliferation. To investigate the capability of PEU-g-nTiO_2/PEUU scaffold to supporting cell growth, bone marrow-derived MSCs were seeded on the scaffold of PEU-g-nTiO_2/PEUU = 1:1 since it had the highest Young's modulus. PEUU and nTiO_2/PEUU scaffolds were used as controls. Bone marrow-derived MSCs are known for their ability to promote bone regeneration. Cell dsDNA (for live cells) content was monitored during the culture. Fig. 9 demonstrated

Table 1
EDX analysis of Ca and P content in the scaffolds after 8 weeks of incubation in SBF.

Element (%)	PEUU	nTiO_2/PEUU	PEU-g-TiO_2/PEUU
Ca	0.039	0.103	0.203
P	0.143	0.327	1.270

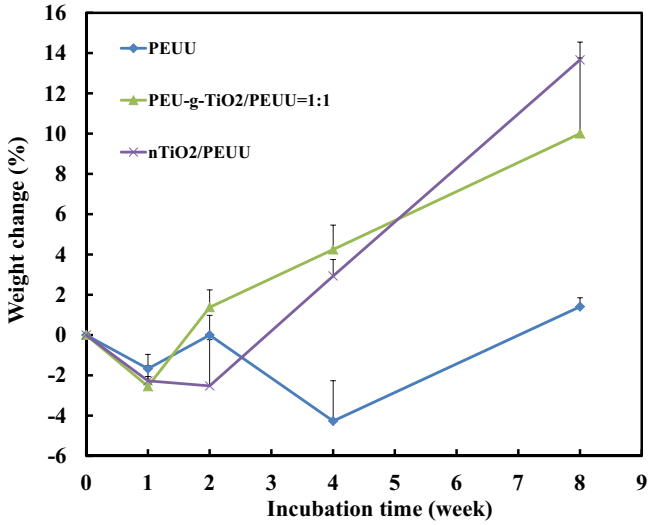

Fig. 7. Weight change of scaffolds incubated in the 37 °C simulated body fluid for 8 weeks.

that MSC dsDNA content was increased on all 3 scaffolds during the 7-day culture period. The highest increase was found for PEU-g-nTiO_2/PEUU scaffold where dsDNA content was 2.5 and 9.9 folds of day 1 at days 3 and 7, respectively ($p < 0.01$ for day 3 vs. day 1, and day 7 vs. day 3). The nTiO_2/PEUU scaffold and PEUU scaffold exhibited similar levels of dsDNA increase at day 7 ($p < 0.05$ for day 7 vs. day 1 for both scaffolds). The above results demonstrate that incorporation of PEU modified TiO_2 nanoparticles into PEUU scaffold improved MSC proliferation while incorporation of unmodified TiO_2 nanoparticles did not. It is possible that PEU on the nanoparticle surface augmented its hydrophilicity, thus increasing its interaction with cells. Our future work will explore how scaffold properties such as TiO_2 content, fiber diameter, and single fiber modulus can be tuned to induce the differentiation of MSCs into osteogenic phenotype.

One of the concerns for using TiO_2 nanoparticles is that the released nanoparticles may be toxic to bone cells [66]. For example, TiO_2 nanoparticles with size of 15 nm have been shown to impair SOD1 and SOD2 secretion and promote ROS generation after intaking by osteoblasts [84]. TiO_2 nanoparticles can also change the ultrastructure of cells [84]. In this work, the PEU modified TiO_2 nanoparticles may not be readily released from the PEUU fibers due to increased interaction between the nanoparticles and PEUU. In addition, the PEU modified TiO_2 nanoparticles may not be easily intaken by the cells even after PEU and PEUU are degraded. Biomineralization study demonstrated that the modified nanoparticles promoted mineral deposition, which can increase the size of the nanoparticles to an extent that cells cannot readily intake.

4. Conclusion

Fibrous PEUU scaffolds reinforced with TiO_2 nanoparticles were fabricated for bone regeneration. Unmodified TiO_2 nanoparticles cannot uniformly distribute in the fibers, and did not show reinforcement effect. The PEU modified nanoparticles can evenly distribute in the fibers, and significantly increased scaffold Young's modulus and tensile strength. The scaffolds based on modified TiO_2 nanoparticles and PEUU exhibited greater biomineralization capability than PEUU scaffold. In addition, these scaffolds better promoted MSC growth than pure PEUU scaffold and PEUU scaffold with unmodified TiO_2 nanoparticles. These scaffolds alone or combined with osteogenic cells have the potential for bone regeneration.

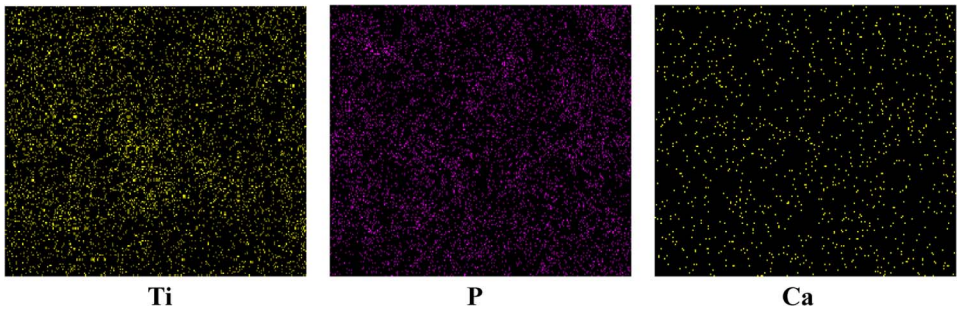

Fig. 8. EDX characterization of Ca and P deposition in the scaffold PEU-g-nTiO$_2$/PEUU = 1:1.

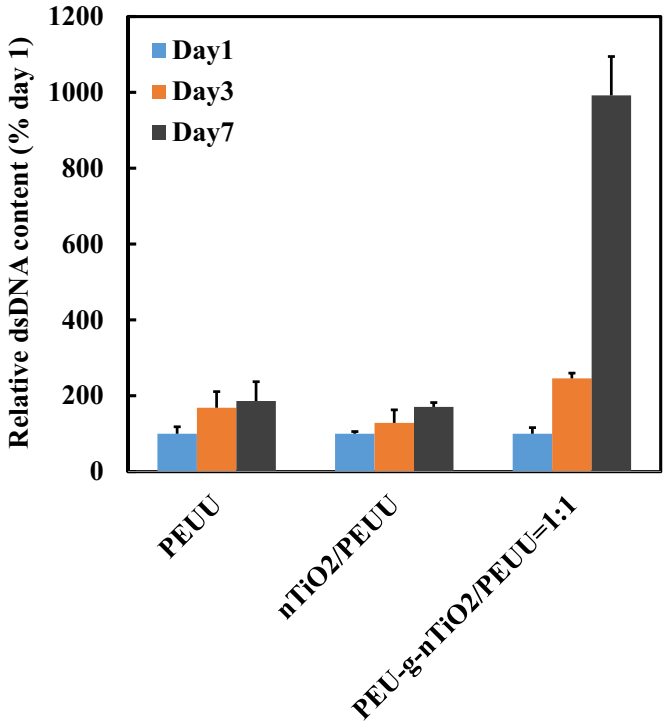

Fig. 9. Mesenchymal stem cell growth on the scaffolds with and without reinforcement with PEU-gnTiO$_2$.

Acknowledgements

This work was supported by US National Institutes of Health (R01HL138353, R01EB022018, R01AG056919, and R21EB021896), US National Science Foundation (1708956), National Science Foundation of China (81471788 and 51462014), Young Scientists of Jiangxi Province (20122BCB23019), “2014 Oceangoing Voyage” from Jiangxi Science and Technology Association, and China Scholarship Council (P-1-00577).

References

[1] N. Mardas, X. Dereka, N. Donos, M. Dard, Experimental model for bone regeneration in oral and cranio-maxillo-facial surgery, J. Investig. Surg. 27 (2014) 32–49.
[2] A.R. Short, D. Koralla, A. Deshmukh, B. Wissel, B. Stocker, M. Calhoun, D. Dean, J.O. Winter, Hydrogels that allow and facilitate bone repair, remodeling, and regeneration, J. Mater. Chem. B Mater. Biol. Med. 3 (2015) 7818–7830.
[3] M. van Griensven, Preclinical testing of drug delivery systems to bone, Adv. Drug Deliv. Rev. 94 (2015) 151–164.
[4] E.A. Abou Neel, L. Bozec, J.C. Knowles, O. Syed, V. Mudera, R. Day, J.K. Hyun, Collagen–emerging collagen based therapies hit the patient, Adv. Drug Deliv. Rev. 65 (2013) 429–456.
[5] A.M. Ferreira, P. Gentile, V. Chiono, G. Ciardelli, Collagen for bone tissue regeneration, Acta Biomater. 8 (2012) 3191–3200.
[6] N. Li, J. Song, G. Zhu, X. Li, L. Liu, X. Shi, Y. Wang, Periosteum tissue engineering-a review, Biomater. Sci. 4 (2016) 1554–1561.
[7] M.G. Raucci, V. Guarino, L. Ambrosio, Biomimetic strategies for bone repair and regeneration, J. Funct. Biomater. 3 (2012) 688–705.
[8] L.C. Gerhardt, G.M. Jell, A.R. Boccaccini, Titanium dioxide (TiO(2)) nanoparticles filled poly(D,L lactid acid) (PDLLA) matrix composites for bone tissue engineering, J. Mater. Sci. Mater. Med. 18 (2007) 1287–1298.
[9] S.M. Giannitelli, F. Basoli, P. Mozetic, P. Piva, F.N. Bartuli, F. Luciani, C. Arcuri, M. Trombetta, A. Rainer, S. Licoccia, Graded porous polyurethane foam: a potential scaffold for oro-maxillary bone regeneration, Mater Sci Eng C Mater Biol Appl 51 (2015) 329–335.
[10] S. Gogoi, S. Maji, D. Mishra, K.S. Devi, T.K. Maiti, N. Karak, Nano-bio engineered carbon dot-peptide functionalized water dispersible hyperbranched polyurethane for bone tissue regeneration, Macromol. Biosci. 17 (2017).
[11] D. Kai, M.P. Prabhakaran, B.Q. Chan, S.S. Liow, S. Ramakrishna, F. Xu, X.J. Loh, Elastic poly(epsilon-caprolactone)-polydimethylsiloxane copolymer fibers with shape memory effect for bone tissue engineering, Biomed. Mater. (Bristol, England) 11 (2016) 015007.
[12] H.Y. Mi, S. Palumbo, X. Jing, L.S. Turng, W.J. Li, X.F. Peng, Thermoplastic polyurethane/hydroxyapatite electrospun scaffolds for bone tissue engineering: effects of polymer properties and particle size, J Biomed Mater Res B Appl Biomater 102 (2014) 1434–1444.
[13] T. Pirvu, S.B. Blanquer, L.M. Benneker, D.W. Grijpma, R.G. Richards, M. Alini, D. Eglin, S. Grad, Z. Li, A combined biomaterial and cellular approach for annulus fibrosus rupture repair, Biomaterials 42 (2015) 11–19.
[14] M. Selvakumar, H.S. Pawar, N.K. Francis, B. Das, S. Dhara, S. Chattopadhyay, Excavating the role of aloe vera wrapped mesoporous hydroxyapatite frame ornamentation in newly architectured polyurethane scaffolds for osteogenesis and guided bone regeneration with microbial protection, ACS Appl. Mater. Interfaces 8 (2016) 5941–5960.
[15] G. Tetteh, A.S. Khan, R.M. Delaine-Smith, G.C. Reilly, I.U. Rehman, Electrospun polyurethane/hydroxyapatite bioactive scaffolds for bone tissue engineering: the role of solvent and hydroxyapatite particles, J. Mech. Behav. Biomed. Mater. 39 (2014) 95–110.
[16] J. Yu, H. Xia, A. Teramoto, Q.Q. Ni, Fabrication and characterization of shape memory polyurethane porous scaffold for bone tissue engineering, J. Biomed. Mater. Res. A 105 (2017) 1132–1137.
[17] C. Zhu, J. Li, C. Liu, P. Zhou, H. Yang, B. Li, Modulation of the gene expression of annulus fibrosus-derived stem cells using poly(ether carbonate urethane)urea scaffolds of tunable elasticity, Acta Biomater. 29 (2016) 228–238.
[18] K.K. Gomez-Lizarraga, C. Flores-Morales, M.L. Del Prado-Audelo, M.A. Alvarez-Perez, M.C. Pina-Barba, C. Escobedo, Polycaprolactone- and polycaprolactone/ceramic-based 3D-bioplotted porous scaffolds for bone regeneration: a comparative study, Mater Sci Eng C Mater Biol Appl 79 (2017) 326–335.
[19] J.H. Kim, M.S. Kang, M. Eltohamy, T.H. Kim, H.W. Kim, Dynamic mechanical and nanofibrous topological combinatory cues designed for periodontal ligament engineering, PLoS One 11 (2016) e0149967.
[20] M. Kim, H.S. Yun, G.H. Kim, Electric-field assisted 3D-fibrous bioceramic-based scaffolds for bone tissue regeneration: fabrication, characterization, and in vitro cellular activities, Sci. Rep. 7 (2017) 3166.
[21] W. Kim, C.H. Jang, G. Kim, Optimally designed collagen/polycaprolactone biocomposites supplemented with controlled release of HA/TCP/rhBMP-2 and HA/TCP/PRP for hard tissue regeneration, Mater Sci Eng C Mater Biol Appl 78 (2017) 763–772.
[22] N. Omidvar, F. Ganji, M.B. Eslaminejad, In vitro osteogenic induction of human marrow-derived mesenchymal stem cells by PCL fibrous scaffolds containing dexamethazone-loaded chitosan microspheres, J. Biomed. Mater. Res. A 104 (2016) 1657–1667.
[23] A.M. Pobloth, H. Schell, A. Petersen, K. Beierlein, C. Kleber, K. Schmidt-Bleek, G.N. Duda, Tubular open-porous beta-TCP-PLCL scaffolds as guiding structure for segmental bone defect regeneration in a novel sheep model, J. Tissue Eng. Regen. Med. (2017), http://dx.doi.org/10.1002/term.2446.
[24] N. Thi Hiep, H. Chan Khon, N. Dai Hai, L. Byong-Taek, V. Van Toi, L. Thanh Hung, Biocompatibility of PCL/PLGA-BCP porous scaffold for bone tissue engineering applications, J. Biomater. Sci. Polym. Ed. 28 (2017) 864–878.
[25] E.J. Adolph, R. Guo, A.C. Pollins, K. Zienkiewicz, N. Cardwell, J.M. Davidson, S.A. Guelcher, L.B. Nanney, Injected biodegradable polyurethane scaffolds support tissue infiltration and delay wound contraction in a porcine excisional model, J Biomed Mater Res B Appl Biomater 104 (2016) 1679–1690.
[26] R. Guo, C.L. Ward, J.M. Davidson, C.L. Duvall, J.C. Wenke, S.A. Guelcher, A transient cell-shielding method for viable MSC delivery within hydrophobic scaffolds polymerized in situ, Biomaterials 54 (2015) 21–33.

[27] A.E. Hafeman, K.J. Zienkiewicz, E. Carney, B. Litzner, C. Stratton, J.C. Wenke, S.A. Guelcher, Local delivery of tobramycin from injectable biodegradable polyurethane scaffolds, J. Biomater. Sci. Polym. Ed. 21 (2010) 95–112.
[28] T. Yoshii, A.E. Hafeman, J.M. Esparza, A. Okawa, G. Gutierrez, S.A. Guelcher, Local injection of lovastatin in biodegradable polyurethane scaffolds enhances bone regeneration in a critical-sized segmental defect in rat femora, J. Tissue Eng. Regen. Med. 8 (2014) 589–595.
[29] T. Yoshii, A.E. Hafeman, J.S. Nyman, J.M. Esparza, K. Shinomiya, D.M. Spengler, G.R. Mundy, G.E. Gutierrez, S.A. Guelcher, A sustained release of lovastatin from biodegradable, elastomeric polyurethane scaffolds for enhanced bone regeneration, Tissue Eng. Part A 16 (2010) 2369–2379.
[30] H.C. Guo, E. Ye, Z. Li, M.Y. Han, X.J. Loh, Recent progress of atomic layer deposition on polymeric materials, Mater Sci Eng C Mater Biol Appl 70 (2017) 1182–1191.
[31] Z. Li, E. Ye, David, R. Lakshminarayanan, X.J. Loh, Recent advances of using hybrid nanocarriers in remotely controlled therapeutic delivery, Small 12 (2016) 4782–4806 (Weinheim an der Bergstrasse, Germany).
[32] X.J. Loh, T.C. Lee, Q. Dou, G.R. Deen, Utilising inorganic nanocarriers for gene delivery, Biomater. Sci. 4 (2016) 70–86.
[33] C.P. Teng, T. Zhou, E. Ye, S. Liu, L.D. Koh, M. Low, X.J. Loh, K.Y. Win, L. Zhang, M.Y. Han, Effective targeted Photothermal ablation of multidrug resistant bacteria and their biofilms with NIR-absorbing gold nanocrosses, Adv. Healthc. Mater. 5 (2016) 2122–2130.
[34] E. Ye, M.D. Regulacio, M.S. Bharathi, H. Pan, M. Lin, M. Bosman, K.Y. Win, H. Ramanarayan, S.Y. Zhang, X.J. Loh, Y.W. Zhang, M.Y. Han, An experimental and theoretical investigation of the anisotropic branching in gold nanocrosses, Nano 8 (2016) 543–552.
[35] E. Ye, M.D. Regulacio, S.Y. Zhang, X.J. Loh, M.Y. Han, Anisotropically branched metal nanostructures, Chem. Soc. Rev. 44 (2015) 6001–6017.
[36] E.Y. Ye, X.J. Loh, Polymeric hydrogels and nanoparticles: a merging and emerging field, Aust. J. Chem. 66 (2013) 997–1007.
[37] Q.Q. Dou, C.P. Teng, E.Y. Ye, X.J. Loh, Effective near-infrared photodynamic therapy assisted by upconversion nanoparticles conjugated with photosensitizers, Int. J. Nanomedicine 10 (2015) 419–432.
[38] E. Ellis, K.Y. Zhang, Q.Y. Lin, E.Y. Ye, A. Poma, G. Battaglia, X.J. Loh, T.C. Lee, Biocompatible pH-responsive nanoparticles with a core-anchored multilayer shell of triblock copolymers for enhanced cancer therapy, J. Mater. Chem. B 5 (2017) 4421–4425.
[39] B.M. Teo, D.J. Young, X.J. Loh, Magnetic anisotropic particles: toward remotely actuated applications, Part. Part. Syst. Charact. 33 (2016) 709–728.
[40] C. Dhand, N. Dwivedi, X.J. Loh, A.N.J. Ying, N.K. Verma, R.W. Beuerman, R. Lakshminarayanan, S. Ramakrishna, Methods and strategies for the synthesis of diverse nanoparticles and their applications: a comprehensive overview, RSC Adv. 5 (2015) 105003–105037.
[41] Q.Q. Dou, X.T. Fang, S. Jiang, P.L. Chee, T.C. Lee, X.J. Loh, Multi-functional fluorescent carbon dots with antibacterial and gene delivery properties, RSC Adv. 5 (2015) 46817–46822.
[42] K. Huang, Q.Q. Dou, X.J. Loh, Nanomaterial mediated optogenetics: opportunities and challenges, RSC Adv. 6 (2016) 60896–60906.
[43] R. Lakshminarayanan, E.O. Chi-Jin, X.J. Loh, R.M. Kini, S. Valiyaveettil, Purification and characterization of a vaterite-inducing peptide, pelovaterin, from the eggshells of *Pelodiscus sinensis* (Chinese soft-shelled turtle), Biomacromolecules 6 (2005) 1429–1437.
[44] R. Lakshminarayanan, X.J. Loh, S. Gayathri, S. Sindhu, Y. Banerjee, R.M. Kini, S. Valiyaveettil, Formation of transient amorphous calcium carbonate precursor in quail eggshell mineralization: an in vitro study, Biomacromolecules 7 (2006) 3202–3209.
[45] A.J. Neumann, M. Alini, C.W. Archer, M.J. Stoddart, Chondrogenesis of human bone marrow-derived mesenchymal stem cells is modulated by complex mechanical stimulation and adenoviral-mediated overexpression of bone morphogenetic protein 2, Tissue Eng. Part A 19 (2013) 1285–1294.
[46] A.J. Neumann, O.F. Gardner, R. Williams, M. Alini, C.W. Archer, M.J. Stoddart, Human articular cartilage progenitor cells are responsive to mechanical stimulation and adenoviral-mediated overexpression of bone-morphogenetic protein 2, PLoS One 10 (2015) e0136229.
[47] A.E. Hafeman, B. Li, T. Yoshii, K. Zienkiewicz, J.M. Davidson, S.A. Guelcher, Injectable biodegradable polyurethane scaffolds with release of platelet-derived growth factor for tissue repair and regeneration, Pharm. Res. 25 (2008) 2387–2399.
[48] Z. Chen, S. Cheng, Z. Li, K. Xu, G.Q. Chen, Synthesis, characterization and cell compatibility of novel poly(ester urethane)s based on poly(3-hydroxybutyrate-co-4-hydroxybutyrate) and poly(3-hydroxybutyrate-co-3-hydroxyhexanoate) prepared by melting polymerization, J. Biomater. Sci. Polym. Ed. 20 (2009) 1451–1471.
[49] J. Guan, K.L. Fujimoto, M.S. Sacks, W.R. Wagner, Preparation and characterization of highly porous, biodegradable polyurethane scaffolds for soft tissue applications, Biomaterials 26 (2005) 3961–3971.
[50] J. Guan, W.R. Wagner, Synthesis, characterization and cytocompatibility of polyurethaneurea elastomers with designed elastase sensitivity, Biomacromolecules 6 (2005) 2833–2842.
[51] Y. Hong, J. Guan, K.L. Fujimoto, R. Hashizume, A.L. Pelinescu, W.R. Wagner, Tailoring the degradation kinetics of poly(ester carbonate urethane)urea thermoplastic elastomers for tissue engineering scaffolds, Biomaterials 31 (2010) 4249–4258.
[52] F. Wang, Z. Li, J.L. Lannutti, W.R. Wagner, J. Guan, Synthesis, characterization and surface modification of low moduli poly(ether carbonate urethane)ureas for soft tissue engineering, Acta Biomater. 5 (2009) 2901–2912.
[53] Q. Wang, C. Chen, W. Liu, X. He, N. Zhou, D. Zhang, H. Gu, J. Li, J. Jiang, W. Huang, Levofloxacin loaded mesoporous silica microspheres/nano-hydroxyapatite/polyurethane composite scaffold for the treatment of chronic osteomyelitis with bone defects, Sci. Rep. 7 (2017) 41808.
[54] W. Yang, S.K. Both, G.J. van Osch, Y. Wang, J.A. Jansen, F. Yang, Performance of different three-dimensional scaffolds for in vivo endochondral bone generation, Eur. Cell. Mater. 27 (2014) 350–364.
[55] B. Das, P. Chattopadhyay, S. Maji, A. Upadhyay, M. Das Purkayastha, C.L. Mohanta, T.K. Maity, N. Karak, Bio-functionalized MWCNT/hyperbranched polyurethane bionanocomposite for bone regeneration, Biomed. Mater. (Bristol, England) 10 (2015) 025011.
[56] Z. Han, H. Kong, J. Meng, C. Wang, S. Xie, H. Xu, Electrospun aligned nanofibrous scaffold of carbon nanotubes-polyurethane composite for endothelial cells, J. Nanosci. Nanotechnol. 9 (2009) 1400–1402.
[57] H.Y. Mi, X. Jing, M.R. Salick, T.M. Cordie, L.S. Turng, Carbon nanotube (CNT) and nanofibrillated cellulose (NFC) reinforcement effect on thermoplastic polyurethane (TPU) scaffolds fabricated via phase separation using dimethyl sulfoxide (DMSO) as solvent, J. Mech. Behav. Biomed. Mater. 62 (2016) 417–427.
[58] S.S. Bakhtiyari, S. Karbasi, A. Monshi, M. Montazeri, Evaluation of the effects of nano-TiO_2 on bioactivity and mechanical properties of nano bioglass-P3HB composite scaffold for bone tissue engineering, J. Mater. Sci. Mater. Med. 27 (2016) 2.
[59] B. Pourmollaabbassi, S. Karbasi, B. Hashemibeni, Evaluate the growth and adhesion of osteoblast cells on nanocomposite scaffold of hydroxyapatite/titania coated with poly hydroxybutyrate, Adv. Biomed. Res. 5 (2016) 156.
[60] D.R. Paul, L.M. Robeson, Polymer nanotechnology: nanocomposites, Polymer 49 (2008) 3187–3204.
[61] A. Borzabadi-Farahani, E. Borzabadi, E. Lynch, Nanoparticles in orthodontics, a review of antimicrobial and anti-caries applications, Acta Odontol. Scand. 72 (2014) 413–417.
[62] L. Cheng, K. Zhang, M.D. Weir, M.A. Melo, X. Zhou, H.H. Xu, Nanotechnology strategies for antibacterial and remineralizing composites and adhesives to tackle dental caries, Nanomedicine (London) 10 (2015) 627–641.
[63] K. Gulati, S. Ivanovski, Dental implants modified with drug releasing titania nanotubes: therapeutic potential and developmental challenges, Expert Opinion on Drug Delivery, 2016, pp. 1–16, , http://dx.doi.org/10.1080/17425247.2017.1266332.
[64] F.U. Rehman, C. Zhao, H. Jiang, X. Wang, Biomedical applications of nano-titania in theranostics and photodynamic therapy, Biomater. Sci. 4 (2016) 40–54.
[65] P.A. Charpentier, K. Burgess, L. Wang, R.R. Chowdhury, A.F. Lotus, G. Moula, Nano-TiO2/polyurethane composites for antibacterial and self-cleaning coatings, Nanotechnology 23 (2012) 425606.
[66] Z. Chen, Y. Wang, T. Ba, Y. Li, J. Pu, T. Chen, Y. Song, Y. Gu, Q. Qian, J. Yang, G. Jia, Genotoxic evaluation of titanium dioxide nanoparticles in vivo and in vitro, Toxicol. Lett. 226 (2014) 314–319.
[67] A.M. Diez-Pascual, A.L. Diez-Vicente, Nano-TiO2 reinforced PEEK/PEI blends as biomaterials for load-bearing implant applications, ACS Appl. Mater. Interfaces 7 (2015) 5561–5573.
[68] I.O. Smith, X.H. Liu, L.A. Smith, P.X. Ma, Nanostructured polymer scaffolds for tissue engineering and regenerative medicine, Wiley Interdiscip. Rev. Nanomed. Nanobiotechnol. 1 (2009) 226–236.
[69] H. Sun, K. Feng, J. Hu, S. Soker, A. Atala, P.X. Ma, Osteogenic differentiation of human amniotic fluid-derived stem cells induced by bone morphogenetic protein-7 and enhanced by nanofibrous scaffolds, Biomaterials 31 (2010) 1133–1139.
[70] J. Wang, X. Liu, X. Jin, H. Ma, J. Hu, L. Ni, P.X. Ma, The odontogenic differentiation of human dental pulp stem cells on nanofibrous poly(L-lactic acid) scaffolds in vitro and in vivo, Acta Biomater. 6 (2010) 3856–3863.
[71] W. Wang, M. Dang, Z. Zhang, J. Hu, T.W. Eyster, L. Ni, P.X. Ma, Dentin regeneration by stem cells of apical papilla on injectable nanofibrous microspheres and stimulated by controlled BMP-2 release, Acta Biomater. 36 (2016) 63–72.
[72] H.M. Borteh, M.D. Gallovic, S. Sharma, K.J. Peine, S. Miao, D.J. Brackman, K. Gregg, Y. Xu, X. Guo, J. Guan, E.M. Bachelder, K.M. Ainslie, Electrospun acetalated dextran scaffolds for temporal release of therapeutics, Langmuir: ACS J. Surf. Colloids 29 (2013) 7957–7965.
[73] X. Guo, C.G. Elliott, Z. Li, Y. Xu, D.W. Hamilton, J. Guan, Creating 3D angiogenic growth factor gradients in fibrous constructs to guide fast angiogenesis, Biomacromolecules 13 (2012) 3262–3271.
[74] F. Wang, Z. Li, K. Tamama, C.K. Sen, J. Guan, Fabrication and characterization of prosurvival growth factor releasing, anisotropic scaffolds for enhanced mesenchymal stem cell survival/growth and orientation, Biomacromolecules 10 (2009) 2609–2618.
[75] Y. Xu, S. Patnaik, X. Guo, Z. Li, W. Lo, R. Butler, A. Claude, Z. Liu, G. Zhang, J. Liao, P.M. Anderson, J. Guan, Cardiac differentiation of cardiosphere-derived cells in scaffolds mimicking morphology of the cardiac extracellular matrix, Acta Biomater. 10 (2014) 3449–3462.
[76] C.L. Zhang, S.H. Yu, Nanoparticles meet electrospinning: recent advances and future prospects, Chem. Soc. Rev. 43 (2014) 4423–4448.
[77] F. Wang, Z. Li, J. Guan, Fabrication of mesenchymal stem cells-integrated vascular constructs mimicking multiple properties of the native blood vessels, J. Biomater. Sci. Polym. Ed. 24 (2013) 769–783.
[78] K.C. Nune, R.D. Misra, S.J. Li, Y.L. Hao, R. Yang, Cellular response of osteoblasts to low modulus Ti-24Nb-4Zr-8Sn alloy mesh structure, J. Biomed. Mater. Res. A 105 (2017) 859–870.
[79] Y. Xu, M. Fu, Z. Li, Z. Fan, X. Li, Y. Liu, P.M. Anderson, X. Xie, Z. Liu, J. Guan, A prosurvival and proangiogenic stem cell delivery system to promote ischemic limb regeneration, Acta Biomater. 31 (2016) 99–113.
[80] Y. Xu, Z. Li, X. Li, Z. Fan, Z. Liu, X. Xie, J. Guan, Regulating myogenic differentiation of mesenchymal stem cells using thermosensitive hydrogels, Acta

Biomater. 26 (2015) 23–33.
[81] M. Gratzel, Solar energy conversion by dye-sensitized photovoltaic cells, Inorg. Chem. 44 (2005) 6841–6851.
[82] Z. Jing, Y. Wu, W. Su, M. Tian, W. Jiang, L. Cao, L. Zhao, Z. Zhao, Carbon nanotube reinforced collagen/hydroxyapatite scaffolds improve bone tissue formation in vitro and in vivo, Ann. Biomed. Eng. (2017), http://dx.doi.org/10.1007/s10439-017-1866-9.
[83] J. Loberg, J. Perez Holmberg, I. Mattisson, A. Arvidsson, E. Ahlberg, Electronic properties of TiO2 nanoparticles films and the effect on apatite-forming ability, Int. J. Dentistry 2013 (2013) 139615.
[84] R. Nogueiras, K.M. Habegger, N. Chaudhary, B. Finan, A.S. Banks, M.O. Dietrich, T.L. Horvath, D.A. Sinclair, P.T. Pfluger, M.H. Tschop, Sirtuin 1 and sirtuin 3: physiological modulators of metabolism, Physiol. Rev. 92 (2012) 1479–1514.